Seasonal temperature variation influences climate suitability for dengue, chikungunya, and Zika transmission

John H. Huber[1, 2], Marissa L. Childs[3], Jamie M. Caldwell[2], Erin A. Mordecai[2*]

[1]Department of Applied and Computational Mathematics and Statistics, University of Notre Dame, Notre Dame, Indiana, USA

[2]Department of Biology, Stanford University, Stanford, California, USA

[3]Emmett Interdisciplinary Program in Environment and Resources, Stanford University, Stanford, California, USA

*Corresponding Author: emordeca@stanford.edu

Short title: Seasonal climate affects vector transmission

ABSTRACT

Dengue, chikungunya, and Zika virus epidemics transmitted by *Aedes aegypti* mosquitoes have recently (re)emerged and spread throughout the Americas, Southeast Asia and the Pacific Islands, and elsewhere. Understanding how environmental conditions affect epidemic magnitude and duration is critical for predicting and responding to the geographic and seasonal spread of disease. Here, we develop the first dynamic disease transmission model for dengue virus and *Aedes aegypti* mosquitoes that integrates mechanistic, empirically parameterized, and independently validated mosquito and virus trait thermal responses under seasonally varying temperatures. With the model, we examine the influence of variation in seasonal temperature regime on epidemic dynamics. We find that at both constant and seasonally varying temperatures, warmer temperatures at the start of epidemics promote more rapid epidemics due to faster burnout of the susceptible population. By contrast, intermediate temperatures (~24°C) at epidemic onset produced the largest epidemics in a seasonally varying temperature regime. When seasonal temperature variation was low, 25-35°C annual average temperatures produced the largest epidemics, but this range shifts to cooler temperatures as seasonal temperature variation increases. Tropical and sub-tropical cities such as Rio de Janeiro, Fortaleza, and Salvador, Brazil; Cali, Cartagena, and Baranquilla, Colombia; Delhi, India; Guangzhou, China; and Manila, Philippines have mean annual temperatures and seasonal temperature ranges that produce the largest epidemics. However, more temperate cities like Shanghai, China had high epidemic suitability because large seasonal variation offset moderate annual

average temperatures. By accounting for seasonal variation in temperature, our model provides a baseline for mechanistically understanding environmental suitability for virus transmission by *Aedes aegypti*. Overlaying the impact of human activities and socioeconomic factors onto this mechanistic temperature-dependent framework is critical for understanding likelihood and magnitude of outbreaks.

NON-TECHNICAL SUMMARY (150-200 WORDS)

Mosquito-borne viruses like dengue, Zika, and chikungunya have recently caused large epidemics that are partly driven by temperature. Using a mathematical model built from laboratory experimental data for *Aedes aegypti* mosquitoes and dengue virus, we examine the impact of variation in seasonal temperature regimes on epidemic size and duration. At constant temperatures, both low and high temperatures (20°C and 35°C) produce small epidemics, while intermediate temperatures like 25°C and 30°C produce much larger epidemics. In seasonally varying temperature environments, epidemics peak more rapidly at higher starting temperatures. Intermediate starting temperatures produce the largest epidemics. Seasonal mean temperatures of 25-35°C are most suitable for large epidemics when seasonality is low, but in more variable seasonal environments epidemic suitability peaks at lower annual average temperatures. Tropical and sub-tropical cities have the highest temperature suitability for epidemics, but more temperate cities with high seasonal variation also have the potential for very large epidemics.

INTRODUCTION

Over the last 30-40 years, arboviral outbreaks have dominated the public health landscape globally (1). These viruses, most notably chikungunya (CHIKV), dengue (DENV), and Zika (ZIKV), can cause symptoms ranging from rash, arthralgia, and fever to hemorrhagic fever (DENV), long-term arthritis (CHIKV), Guillain-Barré syndrome and microcephaly (ZIKV) (2–4). DENV, which historically spread worldwide along shipping routes (5), places 3.97 billion individuals at risk worldwide (6) and causes an estimated 390 million cases annually, including 96 million symptomatic cases (7). CHIKV was introduced into the Americas in December 2013 after an outbreak in St. Martin Island (8). Since then, autochthonous transmission has been reported in 45 countries (9), and 1.3 billion people worldwide are at risk of contracting CHIKV (10). More recently, the ZIKV epidemic in the Americas captured global attention after the World Health Organization (WHO) designated it a Public Health Emergency of International Concern in February 2016 in response to its association with neurological disorders. Following the first reported case in Brazil in May 2015, ZIKV has spread to 48 countries and territories where it is transmitted autochthonously (11). Because DENV, CHIKV, and ZIKV are mostly transmitted by *Aedes aegypti* mosquitoes, they may have similar geographic distributions and risk factors.

Informed public health decisions to limit the spread and magnitude of these arboviral epidemics depend on a robust understanding of transmission dynamics. One mechanistic modeling framework, the Susceptible – Infected – Recovered (SIR) model, has been implemented successfully to model the dynamics of outbreaks of

influenza, measles, and vector-borne diseases such as CHIKV and ZIKV (12–14). This approach tracks virus population dynamics by compartmentalizing individuals by their state in an epidemic (i.e., Susceptible (S), Infected (I), Recovered (R)). This framework can be extended to include additional compartments, such as a latency stage, or to incorporate the dynamics of the mosquito population for vector transmission.

Arbovirus dynamics are strikingly seasonal and geographically restricted to relatively warm climates (15). This arises because several life history traits of the mosquitoes that transmit DENV, CHIKV, and ZIKV are strongly influenced by temperature and seasonality (16–23). For simplicity, many existing models assume static life history traits (14), and those that address seasonal forcing tend to incorporate sinusoidal variation as a single transmission parameter, β (24). However, decades of experimental work have demonstrated strongly nonlinear (often unimodal) relationships between mosquito and pathogen traits and temperature that are not well captured in a single sinusoidal forcing function (25). Efforts by Yang et al. (26,27) addressed the need to include seasonal variation by adopting an SEI-SEIR compartmental framework with time-varying entomological parameters and fitting the model to DENV incidence data in Campinas, Brazil.

Here, we expand upon an SEI-SEIR model (26,27) to incorporate nonlinear, temperature-dependent vector parameters (25). We use the model to evaluate the effect of temperature on epidemic length and size, producing outputs that are more directly comparable to observed epidemics than static measures like R_0 (28). Importantly, we move beyond mean temperature to examine the impact of seasonal

temperature variation on epidemics, by allowing entomological parameters to vary seasonally with temperature. Specifically, we use the model to ask: (1) How does final epidemic size vary across constant temperatures? (2) Under seasonally varying temperatures, how does the temperature at the start of the epidemic affect the final epidemic size and duration? (3) How do temperature mean and seasonal range interact to determine epidemic size? (4) Based on the model, which geographic locations have high epidemic suitability based on climate?

METHODS

Model

Model Framework

We adopted an SEI-SEIR compartmental modeling framework to simulate arboviral transmission by the *Aedes aegypti* vector (Fig. 1). We introduced temperature-dependence into the model by using fitted thermal response curves for the mosquito life history traits provided by Mordecai et al. (25). The full model is:

$$\frac{dS_V}{dt} = EFD(T) * pEA(T) * MDR(T) * N_V * \left(1 - \frac{N_V}{K(T)}\right) - \left(a(T) * pMI(T) * \frac{I_H}{N_H} + \mu(T)\right) * S_V \quad (1)$$

$$\frac{dE_V}{dt} = a(T) * pMI(T) * \frac{I_H}{N_H} * S_V - \left(PDR(T) + \mu(T)\right) * E_V \quad (2)$$

$$\frac{dI_V}{dt} = PDR(T) * E_V - \mu(T) * I_V \quad (3)$$

$$\frac{dS_H}{dt} = -a(T) * b(T) * \frac{I_V}{N_H} * S_H \quad (4)$$

$$\frac{dE_H}{dt} = a(T) * b(T) * \frac{I_V}{N_H} * S_H - \delta * E_H \quad (5)$$

$$\frac{dI_H}{dt} = \delta * E_H - \eta * I_H \quad (6)$$

$$\frac{dR_H}{dt} = \eta * I_H \quad (7)$$

Fig 1 Caption. Compartmental model of transmission. S_H, E_H, I_H, and R_H represent the susceptible, exposed (or latent), infectious, and recovered segments of the human population, respectively. Likewise, S_V, E_V, and I_V represent the susceptible, exposed (or latent), and infectious segments of the mosquito population. Solid arrows signify the directionality of transition from one compartment to the next, and dashed arrows indicate the directionality of transmission.

The SEI portion of the model describes the vector population, where S_V represents the number of susceptible mosquitoes, E_V is the number of mosquitoes in the latency stage, and I_V is the number of infectious mosquitoes. We assumed that *Aedes aegypti* mosquitoes remain infectious until they die. In equations 1-3, *EFD(T)* is the number of eggs laid per female per day, *pEA(T)* is the probability of mosquito egg-to-adult survival, *MDR(T)* is the mosquito egg-to-adult development rate, N_V is the total mosquito population at time *t* (i.e., $S_v + E_v + I_v$), *K(T)* is the carrying capacity for the mosquito population, *a(T)* is the per mosquito biting rate, *pMI(T)* is the probability of mosquito infection per bite on an infectious host, *μ(T)* is the adult mosquito mortality rate, and *PDR(T)* is the parasite development rate. Each life history trait of the *Aedes aegypti* mosquito is a temperature-dependent function fit from experimental laboratory data (Table 1).

143 **Table 1.** Fitted thermal responses for *Aedes aegypti* life history traits. Traits were fit

144 to a Brière $[cT(T-T_0)(T_m-T)^{\frac{1}{2}}]$ or a quadratic $[c(T-T_m)(T-T_0)]$ function where

145 T represents temperature. T_0 and T_m are the critical thermal minimum and

146 maximum, respectively, and c is the rate constant. Thermal responses were fit by

147 (29).

Trait	Definition	Function	Fitted Parameters		
a	Biting rate (day^{-1})	Brière	c = 2.71e-04	T_{min} = 14.67	T_{max} = 41.00
EFD	Eggs laid per female per day	Brière	c = 2.08e-02	T_{min} = 14.06	T_{max} = 32.03
pEA	Probability of mosquito egg-to-adult survival	Quadratic	c = -3.36e-03	T_{min} = 7.68	T_{max} = 38.31
MDR	Mosquito egg-to-adult development rate (day^{-1})	Brière	c = 1.49e-04	T_{min} = 15.12	T_{max} = 37.67
lf	Adult mosquito lifespan (days)	Quadratic	c = -1.24e+00	T_{min} = 16.63	T_{max} = 31.85
b	Probability of mosquito infectiousness	Brière	c = 9.86e-04	T_{min} = 12.05	T_{max} = 32.79
pMI	Probability of mosquito infection	Brière	c = 5.23e-04	T_{min} = 1.51	T_{max} = 34.74
PDR	Virus extrinsic incubation rate (day^{-1})	Brière	c = 1.04e-04	T_{min} = 11.50	T_{max} = 38.97

148

149

150 The SEIR portion of the model describes the human population, where S_H

151 represents the number of susceptible individuals, E_H the number of latent (or

152 exposed) individuals, I_H the number of infectious individuals, and R_H the number of

153 recovered individuals. We assumed a static population size, N_H, that was neither

154 subject to births nor deaths because the human lifespan far exceeds the duration of

155 an epidemic. Further, we binned asymptomatic and symptomatic individuals into a
156 single infectious class since asymptomatic infections have been shown to transmit
157 DENV (30) and exhibit similar viremic profiles as symptomatic patients in CHIKV
158 (31). Based on previous arboviral outbreaks (32,33), we assumed that an infection
159 conferred long-term immunity to an individual. Thus, a previously infectious
160 individual entering the recovered class is protected from subsequent re-infection
161 for the remainder of the epidemic. In the case of dengue, where there are four
162 unique serotypes, we consider single-season epidemics of a single serotype. In
163 equations 4-7, *b(T)* is the probability of human infection per bite by an infectious
164 mosquito, δ^{-1} is the intrinsic incubation period, and η^{-1} is the human infectivity
165 period. Since human components of the transmission cycle are not seasonal, we
166 used constants of 5.9 days for the intrinsic incubation period, $1/\delta$, and 5.0 days for
167 the infectious period, $1/\eta$ (34). All temperature-independent parameter values are
168 given in Table 2.
169
170 **Table 2.** Values of temperature-invariant parameters used in the model, and their
171 sources.

Parameter	Definition	Value	Source
δ^{-1}	Intrinsic incubation period (days)	5.9	(34)
η^{-1}	Human infectivity period (days)	5.0	(34)
I_0^H/N	Proportion of initially infectious humans	0.0025	(34)
I_0^V/M	Proportion of initially infectious mosquitoes	0.015	(34)

M/N	Ratio of mosquitoes-to-humans at 29°C	2.0	(35)

Further, because the lifespan of an adult mosquito is short relative to the timespan of an epidemic, we allowed mosquito birth and death rates to drive population dynamics. Additionally, the birth rate of susceptible mosquitoes was regulated by a temperature-dependent carrying capacity, K (equation 8), which we modeled as a modified Arrhenius equation (36):

$$K(T) = \frac{EFD(T_0) * pEA(T_0) * MDR(T_0) - \mu(T_0)}{EFD(T_0) * pEA(T_0) * MDR(T_0)} * N_m * e^{\frac{-E_A*(T-T_0)^2}{\kappa_B*(T+273)*(T_0+273)}} \quad (8)$$

Here, T_0 is defined as the reference temperature (i.e., the temperature at which the carrying capacity is greatest) in Celsius, N_m is the maximum carrying capacity, and κ_B is Boltzmann constant (8.617 x 10^{-5} eV/K). *EFD* is the number of eggs laid per female per day, *pEA* is the probability of egg-to-adult mosquito survival, *MDR* is the mosquito egg-to-adult development rate, and μ is the adult mosquito mortality rate. We calculated these values for the reference temperature. E_A is the activation energy, which we set to 0.5 and represents the temperature dependence of the carrying capacity, a conservative estimate as we lacked sufficient data on estimates of the carrying capacity of *Aedes aegypti* and its underlying temperature dependence. To convert from Celsius to Kelvin, we incremented the temperature T and the reference temperature T_0 by 273. Equation (8) was adopted from (36) and modified to allow the distribution to be unimodal. We set the reference temperature, T_0, to 29°C, the optimal transmission temperature for *Aedes aegypti* transmission found by Mordecai et al. (25).

Seasonal Forcing

To address seasonality in the model, we allowed temperature to vary over time. We modeled temperature as a sinusoidal curve with a period of 365 days of the form:

$$T(t) = \frac{T_{max} - T_{min}}{2} * \sin\left(\frac{2\pi}{365} t\right) + T_{mean} \tag{9}$$

Here, T_{max}, T_{mean}, and T_{min} represent the average monthly maximum, mean, and minimum temperatures across a calendar year, respectively, and t is measured in days. By modeling temperature as a function of time, we allowed the life history traits of the *Aedes aegypti* vector to vary across time for the duration of the epidemic.

Data

Life History Traits

To incorporate seasonal forcing into the compartmental modeling framework, we used fitted mechanistic thermal response curves (25). Mordecai et al. (25) examined published data on thermal responses for life history traits of the *Aedes aegypti* vector and adopted a Bayesian approach for fitting quadratic ($Q(T)$; Eq. 10) or Brière ($B(T)$; Eq. 11) curves.

$$Q(T) = c * (T - T_{min}) * (T - T_{max}) \tag{10}$$

$$B(T) = c * T * (T - T_{min}) * \sqrt{T_{max} - T} \tag{11}$$

Here, c is a rate constant, T_{min} is the critical temperature minimum, and T_{max} is the critical temperature maximum. Fitted parameters for each of the traits used in the

213 model are provided in Table 1. Consistent with Mordecai et al. (25) we assumed
214 values above and below the critical thermal maxima and minima, respectively, were
215 equal to zero. By doing so, we constrained the distribution of each life history trait
216 to biologically relevant and empirically driven measures.

217 Mordecai et al. (25) provided a fitted thermal response for adult mosquito
218 lifespan (Table 1), which is equal to the inverse of the adult mosquito mortality rate
219 (μ), in days^{-1}, used in our model. At temperatures greater than or equal to the
220 critical thermal maximum and less than or equal to the critical thermal minimum,
221 adult mosquito mortality was set to 24 days^{-1} (i.e., mosquitoes survive for one hour
222 at temperatures outside of the T_{min} to T_{max} range).

223

224 *Historical Weather Data*

225 To identify areas of epidemic suitability across the globe, we extracted
226 monthly mean temperatures for 2016 from Weather Underground
227 (wunderground.com) for twenty different cities (Table 3). For each city, we
228 calculated the mean, minimum, and maximum from the average monthly mean
229 temperatures, to estimate temperature seasonality. This provided a range of the
230 average monthly temperature over the span of a calendar year. We chose this time
231 period because it provided the most recent full calendar year to demonstrate
232 seasonal fluctuations in temperature.

233

234 **Table 3.** Estimates of epidemic suitability for major cities. Epidemic suitability was
235 calculated as the proportion of the population that became infected in simulations

run under default conditions (see Appendix). Each city was simulated with its respective temperature regime from the 2016 calendar year.

City	Annual Mean Temperature (°C)	Annual Temperature Amplitude (°C)	Epidemic Suitability
Buenos Aires, Argentina	16.5	8.0	0.0313
Sao Paulo, Brazil	20.6	5.0	0.509
Rio de Janeiro, Brazil	24.3	4.0	0.999
Salvador, Brazil	26.3	2.0	0.998
Fortaleza, Brazil	27.8	0.50	0.999
Belo Horizonte, Brazil	21.9	3.0	0.499
Recife, Brazil	27.2	1.5	0.999
Shanghai, China	17.6	12.5	0.993
Beijing, China	12.8	16	0.405
Guangzhou, China	22.9	8.0	0.999
Bogotá, Colombia	14.7	1.0	0.0025
Medellin, Colombia	17.9	1.0	0.00484
Cali, Colombia	25.1	1.5	0.986
Barranquilla, Colombia	28.8	1.0	1.00
Cartagena, Colombia	28.6	1.0	1.00
Delhi, India	26.3	9.5	0.926
Tokyo, Japan	17.0	10.5	0.621

Kobe, Japan	17.4	11	0.899
Manila, Philippines	29.0	1.5	1.00
New York, USA	13.8	12	0.0328

Variability in Epidemic Dynamics with Constant Temperature

We first examined how epidemic dynamics varied across different constant temperatures. Here, we did not introduce seasonal forcing into the model but rather assumed static life history traits for *Aedes aegypti* for the simulation period. We simulated the model under default starting conditions (see Appendix) at different constant temperatures ranging from 0.0°C to 40.0°C in increments of 0.1°C.

Variability in Epidemic Dynamics with Starting Temperature

Using the model that included seasonal variation in temperature, we examined how the dynamics of an epidemic varied due to the temperature at which the epidemic began under two temperature regimes. To address this variation, we set T_{max} = 40.0°C, T_{mean} = 25.0°C, and T_{min} = 10.0°C in the time-varying seasonal temperature model under default parameters provided in the Appendix. We then varied the temperature at the start of the epidemic from 10.0°C to 40.0°C in increments of 0.1°C and examined the response of final epidemic size, epidemic length, and maximum number of infected individuals at any given point in time. We then considered the temperature regime with T_{max} = 30.0°C, T_{mean} = 25.0°C, and T_{min} = 20.0°C. The same metrics were computed using the time-varying seasonal

temperature module with the same parameterization while varying the start of the epidemic from 20.0°C to 30.0°C in increments of 0.1°C

Seasonal Variability of Final Epidemic Size

Using the compartmental modeling framework with the default starting conditions, we examined the variation in final epidemic size as a result of seasonal forcing. To do so, we simulated over a wide range of temperature mean and seasonal variance regimes. The mean annual temperature varied from 0.0°C to 40.0°C in increments of 0.1°C, while the seasonal fluctuation about the mean (i.e., $\frac{T_{max}-T_{min}}{2}$) ranged from 0.0°C to 20.0°C in increments of 0.1°C. Many of these temperature regimes are unlikely to be observed empirically. However, the simulated temperature regimes spanned the full range of feasible temperature conditions. We recorded the final epidemic size, measured as the number of individuals in the recovered compartment at the end of the simulation, for each unique combination of mean annual temperature and seasonal fluctuation.

We then compared simulated climate regimes with actual climates in major cities, to measure relative epidemic suitability of the following cities: São Paulo, Brazil; Rio de Janeiro, Brazil; Salvador, Brazil; Fortaleza, Brazil; Belo Horizonte, Brazil; Recife, Brazil; Bogotá, Colombia; Medellín, Colombia; Cali, Colombia; Barranquilla, Colombia; Cartagena, Colombia; Tokyo, Japan; Delhi, India; Manila, Philippines; Shanghai, China; Beijing, China; New York City, USA; Guangzhou, China; Kobe, Japan; and Buenos Aires, Argentina. These cities were chosen because they

280 represent some of the most populous urban areas across South America and
281 throughout the world.
282
283
284 **Model Sensitivity and Uncertainty Analysis**
285 To characterize uncertainty in the model, we simulated epidemic suitability at a
286 constant temperature, ranging from 0.0°C to 40.0°C in increments of 0.5°C, while
287 sampling 1,000 estimates for c, T_{min}, and T_{max} for each life history trait from the
288 marginal posterior distributions provided by Mordecai et al. (25). We calculated the
289 95% credible interval for the epidemic suitability at each temperature.
290
291 **RESULTS**
292 **Variability in Epidemic Dynamics with Constant Temperature**
293 Holding temperature constant, we examined variability in epidemic dynamics
294 across four temperatures: 20°C, 25°C, 30°C, and 35°C. As temperature increased
295 from 20°C to 30°C, the number of susceptible individuals depleted more rapidly
296 (Fig. 2, S_H). At 20°C and 35°C, the epidemics were small and burned out rapidly.
297 Although simulations run at 25°C and 30°C produced similar final epidemic sizes of
298 92.96% vs. 99.95% of the population infected, respectively (Fig. 2, R_H), the epidemic
299 peaked much faster at 30°C. Finally, smaller epidemics of 1.51% and 6.17% of the
300 population infected occurred at 20°C and 35°C.
301

Fig 2 Caption. Variation in epidemic dynamics by temperature. The model was simulated under default parameters at four constant temperatures: 20°C, 25°C, 30°C, and 35°C. The number of humans in each compartment is represented on a log scale.

Variability in Epidemic Dynamics with Starting Temperature

Next, we examined variability in epidemic dynamics due to the temperature at which the epidemic began, given two fixed temperature regimes (25°C mean and amplitude of either 5°C or 15°C). Consequently, starting temperature was allowed to vary from 10°C to 40°C or 20°C to 30°C depending on the regime.

Given that an epidemic occurred, epidemic length monotonically decreased as a function of starting temperature for both temperature regimes (Fig. 3): warmer temperatures at the start of the epidemic produced shorter epidemics, and vice versa. When temperature varied from 10°C to 40°C, the longest epidemic simulated was 134.97 days and occurred at starting temperatures of 11.3°C and 11.4°C, and the shortest epidemic lasted 16.09 days and occurred when the temperature at the epidemic start was less than 10.3°C. When the temperature was 35.9°C or higher, no epidemic was observed. Similarly, when temperature was constrained between 20°C and 30°C, the longest epidemic simulated was 112.9 days at a starting temperature of 20°C, and the shortest epidemic lasted 71.3 days at a starting temperature of 30°C.

Fig 3 Caption. Epidemiological indices as a function of starting temperature, within a given seasonal temperature regime. The red curve represents the maximum number of humans in the infected class (I_H) at any given point during the simulation. The blue curve represents the final (or cumulative) epidemic size (R_H at the final time step). The green curve represents the length of the epidemic (i.e., the point at which the number of infected individuals was below one). Here, simulations were run with the temperature conditions: T_{min} = 10°C, T_{mean} = 25°C, and T_{max} = 40°C (A) and T_{min} = 20°C, T_{mean} = 25°C, and T_{max} = 30°C (B).

In contrast to epidemic length, both final epidemic size and maximum infected responded unimodally to the temperature at the epidemic onset. The total number of people infected peaked at a starting temperature of 24.1°C for both temperature regimes (Fig. 3). The maximum instantaneous number of infected individuals peaked at 24.4°C in both temperature regimes, with 8.42% of the population infected. Together, these results show that epidemics introduced at different times within identical seasonal temperature regimes produce dramatically different final sizes and maximum infection rates.

Seasonal Variability of Final Epidemic Size

To address how mean temperature and seasonal variance combined to influence the final epidemic size, we simulated over a wide range of temperature regimes that accounted for variation in the mean and temperature range over a calendar year.

347 We calculated relative epidemic suitability, defined as the final epidemic size as a
348 proportion of the human population, for twenty major cities worldwide (Table 3).
349 In a constant thermal environment, a band of mean temperatures between
350 approximately 25°C and 35°C supports the highest epidemic suitability (Fig. 4). As
351 the seasonal temperature range increases, lower mean temperatures are capable of
352 supporting large epidemics. However, outside this narrow band of temperature
353 regimes, epidemic suitability rapidly diminishes and most temperature regimes did
354 not produce epidemics.
355
356 **Fig 4 Caption. Variation in epidemic suitability across different seasonal**
357 **temperature regimes.** The heat map shows the epidemic suitability (represented
358 as the proportion of the total human population infected during an epidemic) as a
359 function of mean annual temperature and temperature range. Here, temperature
360 range is defined as the seasonal fluctuation about the annual mean temperature.
361 Twenty large, globally important cities are plotted to illustrate their epidemic
362 suitability.
363
364 Of the focal 20 major cities, those with high mean temperature and small
365 average temperature fluctuations exhibited the highest epidemic suitability. For
366 instance, Manila, Philippines, which has a monthly mean temperature of 29°C and
367 average seasonal amplitude in mean temperature of 1.50°C, had an epidemic
368 suitability of 1.00. Cartagena and Barranquilla, Colombia also had epidemic
369 suitability of 1.00. On the other hand, areas with low average temperature and

370 greater temperature fluctuations, such as Beijing and New York, exhibited lower—
371 but still non-zero—epidemic suitabilities of 0.405 and 0.0328 respectively. Notably,
372 Guangzhou and Shanghai, China have high epidemic suitability (0.999 and 0.993,
373 respectively) despite high seasonal variation in temperature due to more moderate
374 mean temperatures (22.9 and 17.6°C, respectively), while high seasonal variation
375 reduced suitability to 0.926 in Delhi, India, which has a high mean temperature of
376 26.3°C (Fig. 4).
377
378 **Model Sensitivity and Uncertainty Analysis**
379 Within the 95% credible interval previously estimated for each trait thermal
380 response (25), epidemic suitability as a function of temperature is not highly
381 sensitive to the values of c, T_{min}, and T_{min} (Fig. 5). The 95% credible interval on
382 epidemic suitability across a range of constant temperatures is narrow, suggesting
383 low uncertainty in the predicted final epidemic sizes arising from trait thermal
384 responses.
385
386 **Fig 5 Caption. Sensitivity of epidemic suitability to the parameterization of life**
387 **history traits.** Epidemic suitability (represented as the proportion of the total
388 human population infected during an epidemic) as a function of a constant
389 temperature. Temperature was held constant, and 1,000 samples of c, T_{min}, and T_{max}
390 were taken from the marginal posterior distribution of each trait thermal response
391 from Mordecai et al. (25). The 95% credible interval is represented by the shaded
392 blue region, and the median is plotted in blue.

DISCUSSION

Recent outbreaks of DENV, CHIKV, and ZIKV in Latin America and across the globe have captured the attention of the public health community and underscore the importance of preparation for future outbreaks. As temperatures rise, the global landscape suitable for such outbreaks will expand and shift geographically, potentially placing a larger proportion of the world's population at risk. Understanding how local temperature regimes govern epidemic dynamics becomes increasingly important in resource allocation and control interventions (37).

Epidemic duration and size (i.e., proportion of individuals who eventually become infected) are two key metrics of epidemic dynamics. We explored how epidemic size and duration varied across temperature regimes by extending a mechanistic modeling framework developed by (26) to incorporate nonlinear thermal responses of vector traits and seasonal forcing (25). We found that the temperature mean, seasonal variation, and seasonal timing of epidemic onset differentially affected epidemic size versus duration.

The most notable variation in epidemic dynamics at constant temperature was in the rate at which susceptible individuals were depleted. Epidemics simulated at 25°C and 30°C produced similar final epidemic sizes despite the epidemic at 25°C proceeding at a much slower rate. This "slow burn" phenomenon occurs because slower depletion of susceptible individuals can produce epidemics of similar size to epidemics that infect people very rapidly.

415 Within a given seasonal temperature regime, epidemic size peaked at
416 intermediate starting temperatures (24.1°C for the regimes simulated here). More
417 generally, the unimodal relationship suggests that even in highly suitable seasonal
418 environments, epidemics may vary dramatically depending on when they begin.
419 Compared to epidemic size, the maximum number of infected individuals at a time
420 peaked at slightly higher intermediate starting temperatures. We attribute this
421 difference between the optimal temperatures for final epidemic size and the
422 maximum number of infected individuals to the "slow burn" phenomenon: larger
423 epidemics occurred at slightly lower starting temperatures than the instantaneous
424 maximum number of people infected because the former epidemics last longer.
425 Epidemic suitability was sensitive to the interaction between annual mean
426 temperatures and seasonal temperature variation. At low seasonal amplitude, we
427 found a narrow band of annual mean temperatures (approximately 25-35°C) with
428 the highest epidemic suitability. Outside this band of temperature regimes,
429 suitability diminishes rapidly. Larger seasonal variation in temperature lowers the
430 range of optimal annual mean temperatures (i.e., suitability is high in cooler places
431 with larger seasonal variation in temperature). It is important to note that these
432 epidemic suitabilities should be treated as an upper bound on the potential for large
433 epidemics. That is, within highly suitable climate regimes, epidemics can vary in
434 magnitude due to human population size and movement dynamics (38), effective
435 vector control, and other mitigating factors. Likewise, our estimates are conditioned
436 on an *Aedes aegypti* population being present and virus introduction to support an
437 outbreak.

Previous modeling efforts have addressed seasonal forcing by allowing transmission parameters to vary sinusoidally (24). This assumption of sinusoidal variation does not fully capture the nonlinear relationship between vector traits and temperature. Our mechanistic modeling framework provides the most comprehensive treatment of nonlinear, seasonally varying temperature-dependence for *Ae. aegypti* virus transmission to date. To do so, it incorporates experimentally measured thermal responses for all transmission-relevant vector traits into a dynamic transmission model, and these traits are forced with realistic seasonal temperature variation. To aid future studies in adopting this framework, code is available online to reproduce our results and to expand on this seasonal arboviral transmission model. Accurately describing epidemic dynamics of emerging and established vector-borne pathogens will ultimately require integrating realistic models of environmental suitability, as presented here, with demographic, social, and economic factors that promote or limit disease transmission (39) .

ACKNOWLEDGEMENTS

JHH and EAM were funded by the National Science Foundation (DEB-1518681). EAM was also funded by NSF (DEB-1640780) and the Stanford University Center for Innovation in Global Health. EAM and JMC were funded by the Stanford University Woods Institute for the Environment, Environmental Ventures Program. MLC acknowledges funding from the Lindsay Family E-IPER Fellowship.

REFERENCES

1. Gubler DJ. The Global Emergence / Resurgence of Arboviral Diseases As Public Health Problems. Arch Med Search. 2002;33:330–42.
2. Faria NR, Azevedo R do S da S, Kraemer MUG, Souza R, Cunha MS, Hill SC, et al. Zika virus in the Americas: Early epidemiological and genetic findings. Science [Internet]. 2016;5036(March):aaf5036. Available from: http://science.sciencemag.org/content/early/2016/03/23/science.aaf5036.abstract
3. Staples JE, Breiman RF, Powers AM. Chikungunya Fever: An Epidemiological Review of a Re-Emerging Infectious Disease. Clin Infect Dis [Internet]. 2009;49(6):942–8. Available from: http://cid.oxfordjournals.org/lookup/doi/10.1086/605496
4. World Health Organization (WHO) Regional Office for South-East Asia. Dengue: guidelines for diagnosis, treatment, prevention, and control. Special Programme for Research and Training in Tropical Diseases. 2009.
5. Gubler DJ. Dengue/dengue haemorrhagic fever: history and current status. Novartis Found Symp [Internet]. 2006;277:3-16-22, 71–3, 251–3. Available from: http://europepmc.org/abstract/MED/17319151
6. Brady OJ, Gething PW, Bhatt S, Messina JP, Brownstein JS, Hoen AG, et al. Refining the Global Spatial Limits of Dengue Virus Transmission by Evidence-Based Consensus. PLoS Negl Trop Dis. 2012;6(8).
7. Bhatt S, Gething PW, Brady OJ, Messina JP, Farlow AW, Moyes CL, et al. The global distribution and burden of dengue. Nature [Internet]. 2013;496(7446):504–7. Available from: http://dx.doi.org/10.1038/nature12060
8. Khan K, Bogoch I, Brownstein JS, Miniota J, Nicolucci A, Hu W, et al. Assessing the origin of and potential for international spread of chikungunya virus from the Caribbean. PLoS Curr [Internet]. 2014;6:1–11. Available from: http://www.pubmedcentral.nih.gov/articlerender.fcgi?artid=4055609&tool=pmcentrez&rendertype=abstract
9. Perkins TA, Metcalf CJE, Grenfell BT, Tatem AJ. Estimating drivers of autochthonous transmission of Chikungunya virus in its invasion of the Americas. PLoS Curr. 2015;7(OUTBREAKS):1–26.
10. Nsoesie EO, Kraemer MUG, Golding N, Pigott DM, Brady OJ, Moyes CL, et al. Global distribution and environmental suitability for chikungunya virus, 1952 to 2015. Eurosurveillance. 2016;21(20).
11. PAHO. Regional Zika Epidemiological Update (Americas) August 25, 2017 [Internet]. Pan American Health Organization. 2017 [cited 2017 Dec 4]. Available from: http://www.paho.org/hq/index.php?option=com_content&view=article&id=11599:regional-zika-epidemiological-update-americas&Itemid=41691&lang=en
12. Bjornstad ON, Finkenstadt BF, Grenfell BT. Dynamics of measles epidemics: Estimating scaling of transmission rates using a Time series SIR model. Ecol Monogr. 2002;72(2):169–84.
13. Coburn BJ, Wagner BG, Blower S. Modeling influenza epidemics and pandemics: insights into the future of swine flu (H1N1). BMC Med [Internet]. 2009;7(1):30. Available from: http://bmcmedicine.biomedcentral.com/articles/10.1186/1741-7015-7-30
14. Kucharski AJ, Funk S, Eggo RM, Mallet H, Edmunds WJ, Nilles EJ. Transmission dynamics of Zika virus in island populations : a modelling analysis of the 2013 – 14 French Polynesia outbreak. bioRxiv. 2016;1–15.
15. Ryan SJ, McNally A, Johnson LR, Mordecai EA, Ben-Horin T, Paaijmans K, et al. Mapping Physiological Suitability Limits for Malaria in Africa Under Climate Change. Vector-Borne Zoonotic Dis [Internet]. 2015;15(12):718–25. Available from: http://online.liebertpub.com/doi/10.1089/vbz.2015.1822
16. Eisen L, Monaghan AJ, Lozano-Fuentes S, Steinhoff DF, Hayden MH, Bieringer PE. The impact of temperature on the bionomics of Aedes (Stegomyia) aegypti, with special reference to the cool geographic range margins. J Med Entomol [Internet]. 2014;51(3):496–516. Available

513 from: http://www.ncbi.nlm.nih.gov/pubmed/24897844
514 17. Rueda LM, Patel KJ, Axtell RC, Stinner RE. Temperature-Dependent Development and Survival
515 Rates of Culex quinquefasciatus and Aedes aegypti (Diptera: Culicidae). J Med Entomol
516 [Internet]. 1990;27(5):892–8. Available from: https://academic.oup.com/jme/article-
517 lookup/doi/10.1093/jmedent/27.5.892
518 18. Tun-Lin W, Burkot TR, Kay BH. Effects of temperature and larval diet on development rates
519 and survival of the dengue vector Aedes aegypti in north Queensland, Australia. Med Vet
520 Entomol. 2000;14(1):31–7.
521 19. Kakimura K, Matsuse IT, Takahashi H, Fukuda T, Suzuki K, Aratani M, et al. Effect of
522 temperature on the development of Aedes aegypti and Aedes albopictus. Med Entomol Zool.
523 2002;53(1):53–8.
524 20. Beserra EB, Fernandes CRM, Silva SA de O, Silva L a. Da, Santos JW Dos. Efeitos da
525 temperatura no ciclo de vida, exigências térmicas e estimativas do número de gerações anuais
526 de Aedes aegypti (Diptera, Culicidae). Iheringia Série Zool [Internet]. 2009;99(2):142–8.
527 Available from: http://www.scielo.br/scielo.php?script=sci_arttext&pid=S0073-
528 47212009000200004&lng=pt&nrm=iso&tlng=pt
529 21. Couret J, Dotson E, Benedict MQ. Temperature, larval diet, and density effects on development
530 rate and survival of Aedes aegypti (Diptera: Culicidae). PLoS One. 2014;9(2).
531 22. Watts DM, Burke DS, Harrison BA, Whitmire RE, Nisalak A. Effect of temperature on the
532 vector efficiency of Aedes aegypti for dengue 2 virus. Am J Trop Med Hyg. 1987;36(1):143–
533 52.
534 23. McLean DM, Clarke AM, Coleman JC, Montalbetti CA, Skidmore AG, Walters TE, et al. Vector
535 capability of *Aedes aegypti* mosquitoes for California encephalitis and dengue viruses at
536 various temperatures. Can J Microbiol [Internet]. 1974;20(2):255–62. Available from:
537 http://www.nrcresearchpress.com/doi/abs/10.1139/m74-040
538 24. Altizer S, Dobson A, Hosseini P, Hudson P, Pascual M, Rohani P. Seasonality and the dynamics
539 of infectious diseases: Seasonality and infectious diseases. Ecol Lett. 2006 Mar;9(4):467–84.
540 25. Mordecai EA, Cohen JM, Evans M V., Gudapati P, Johnson LR, Lippi CA, et al. Detecting the
541 impact of temperature on transmission of Zika, dengue, and chikungunya using mechanistic
542 models. PLoS Negl Trop Dis. 2017;11(4).
543 26. Yang HM, Macoris MLG, Galvani KC, Andrighetti MTM, Wanderley DM V. Assessing the effects
544 of temperature on dengue transmission. Epidemiol Infect. 2009;137(8):1179–87.
545 27. Yang HM, Boldrini JL, Fassoni AC, Freitas LFS, Gomez MC, Lima KKB de, et al. Fitting the
546 Incidence Data from the City of Campinas, Brazil, Based on Dengue Transmission Modellings
547 Considering Time-Dependent Entomological Parameters. PLoS One [Internet].
548 2016;11(3):e0152186. Available from: http://dx.plos.org/10.1371/journal.pone.0152186
549 28. Heffernan JM, Smith RJ, Wahl LM. Perspectives on the basic reproductive ratio. J R Soc
550 Interface. 2005;2(4):281–93.
551 29. Mordecai E, Cohen J, Evans M V, Gudapati P, Johnson LR, Miazgowicz K, et al. Temperature
552 determines Zika, dengue and chikungunya transmission potential in the Americas. 2016 Jul.
553 Report No.: biorxiv;063735v1.
554 30. Duong V, Lambrechts L, Paul RE, Ly S, Lay RS, Long KC, et al. Asymptomatic humans transmit
555 dengue virus to mosquitoes. Proc Natl Acad Sci [Internet]. 2015;112(47):14688–93. Available
556 from: http://www.pnas.org/lookup/doi/10.1073/pnas.1508114112
557 31. Appassakij H, Khuntikij P, Kemapunmanus M, Wutthanarungsan R, Silpapojakul K. Viremic
558 profiles in asymptomatic and symptomatic chikungunya fever: A blood transfusion threat?
559 Transfusion. 2013;53(10 PART 2):2567–74.
560 32. Murphy BR, Whitehead SS. Immune Response to Dengue Virus and Prospects for a Vaccine.
561 Annu Rev Immunol [Internet]. 2011;29(1):587–619. Available from:
562 http://www.annualreviews.org/doi/10.1146/annurev-immunol-031210-101315
563 33. Weaver SC, Osorio JE, Livengood JA, Chen R, Stinchcomb DT. Chikungunya virus and
564 prospects for a vaccine. Expert Rev Vaccines [Internet]. 2012;11(9):1087–101. Available
565 from: http://www.tandfonline.com/doi/full/10.1586/erv.12.84
566 34. Kucharski AJ, Funk S, Eggo RM, Mallet H-P, Edmunds WJ, Nilles EJ. Transmission Dynamics of
567 Zika Virus in Island Populations: A Modelling Analysis of the 2013–14 French Polynesia

Outbreak. Barker CM, editor. PLoS Negl Trop Dis. 2016 May;10(5):e0004726.

35. Le Menach A, McKenzie FE, Flahault A, Smith DL. The unexpected importance of mosquito oviposition behaviour for malaria: non-productive larval habitats can be sources for malaria transmission. Malar J [Internet]. 2005;4:23. Available from: http://www.pubmedcentral.nih.gov/articlerender.fcgi?artid=1164431&tool=pmcentrez&rendertype=abstract

36. Palamara GM, Childs DZ, Clements CF, Petchey OL, Plebani M, Smith MJ. Inferring the temperature dependence of population parameters: The effects of experimental design and inference algorithm. Ecol Evol. 2014;4(24):4736–50.

37. Perkins TA. Retracing Zika's footsteps across the Americas with computational modeling. Proc Natl Acad Sci [Internet]. 2017;114(22):5558–60. Available from: http://www.pnas.org/lookup/doi/10.1073/pnas.1705969114

38. Wesolowski A, Qureshi T, Boni MF, Sundsøy PR, Johansson MA, Rasheed SB, et al. Impact of human mobility on the emergence of dengue epidemics in Pakistan. Proc Natl Acad Sci [Internet]. 2015;112(38):11887–92. Available from: http://www.pnas.org/lookup/doi/10.1073/pnas.1504964112

39. Zhang Q, Sun K, Chinazzi M, Pastore y Piontti A, Dean NE, Rojas DP, et al. Spread of Zika virus in the Americas. Proc Natl Acad Sci [Internet]. 2017;114(22):E4334–43. Available from: http://www.pnas.org/lookup/doi/10.1073/pnas.1620161114

40. R Development Core Team. R: A Language and Environment for Statistical Computing [Internet]. Vienna, Austria: R Foundation for Statistical Computing; 2014. Available: http://www.R-project.org

593 **APPENDIX**

594 *Starting Conditions*

595 The model requires estimates of the mosquito-to-human ratio and the
596 number of initially infectious humans and vectors to initiate each simulation. For
597 these initial conditions, we used measures provided in previous models. In a model
598 of the ZIKV outbreak in French Polynesia from 2013-2014, Kucharski et al. provided
599 marginal posterior estimates for the proportion of initially infectious mosquitoes
600 and the number of initially infectious humans on each island (34). We digitized the
601 data for Tahiti and calculated the weighted average to arrive at estimates of 0.015
602 for the proportion of initially infectious vectors. Kucharski et al. estimated the mean
603 number of initially infectious humans to be 450 (34). Assuming the 2012 population
604 size of 183,645 for Tahiti, we arrived at an estimate of 0.0025 for the proportion of
605 initially infectious humans.

606 The literature on the ratio of mosquitoes to humans is limited. One model
607 (35) that measured mosquito oviposition behavior adopted a patch modeling
608 framework in which the overall ratio of mosquitoes to humans was equal to two,
609 which we adopted here.

610 With estimates for the mosquito-to-human ratio and the number of initially
611 infectious individuals and vectors, we were able to calibrate our model. The total
612 human population size, N_H, was set to a constant 10,000. Based on the proportion
613 derived from (34), 25 individuals were initially infectious and the remaining
614 population (9,975 individuals) was completely susceptible. E_H and R_H were initially
615 set to zero.

Since the carrying capacity and adult mosquito mortality rate were both dependent on temperature, the mosquito population size was subject to temperature effects. We assumed that the carrying capacity was greatest at 29°C (based on studies by Mordecai et al., 2016 and Le Menach et al., 2005) and totaled 20,000. To equilibrate the model, we set the initial mosquito population size (M_0) to the carrying capacity calculated from eq. 8 at the starting temperature. The quantity of initially infectious mosquitoes was calculated as 1.5% of the starting population size (34). The remaining mosquitoes (98.5%) were susceptible. The initial conditions were thus:

$$(S_V, E_V, I_V, S_H, E_H, I_H, R_H)_0 = (0.985M_0, 0, 0.015M_0, 9975, 0, 25, 0)$$

Simulations

Simulations were performed using a temperature-sensitive mechanistic modeling framework developed in C++. Code and supporting documentation for this model can be accessed at https://github.com/jhuber3/temperature-sensitive-sir. Simulation outputs were processed in the R Programming Language 4.3.1 (40).

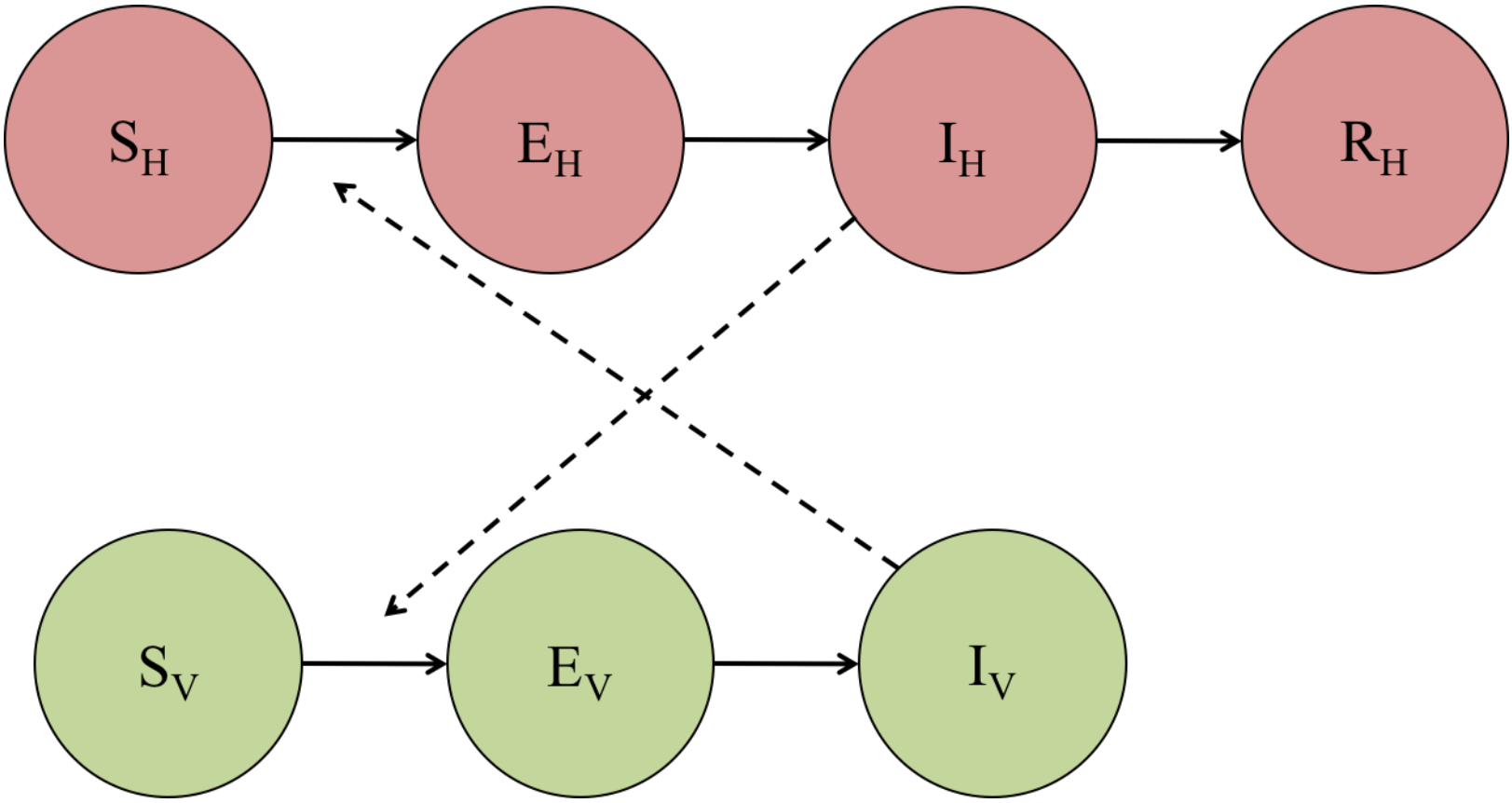
S_H
E_H
I_H
R_H
S_V
E_V
I_V

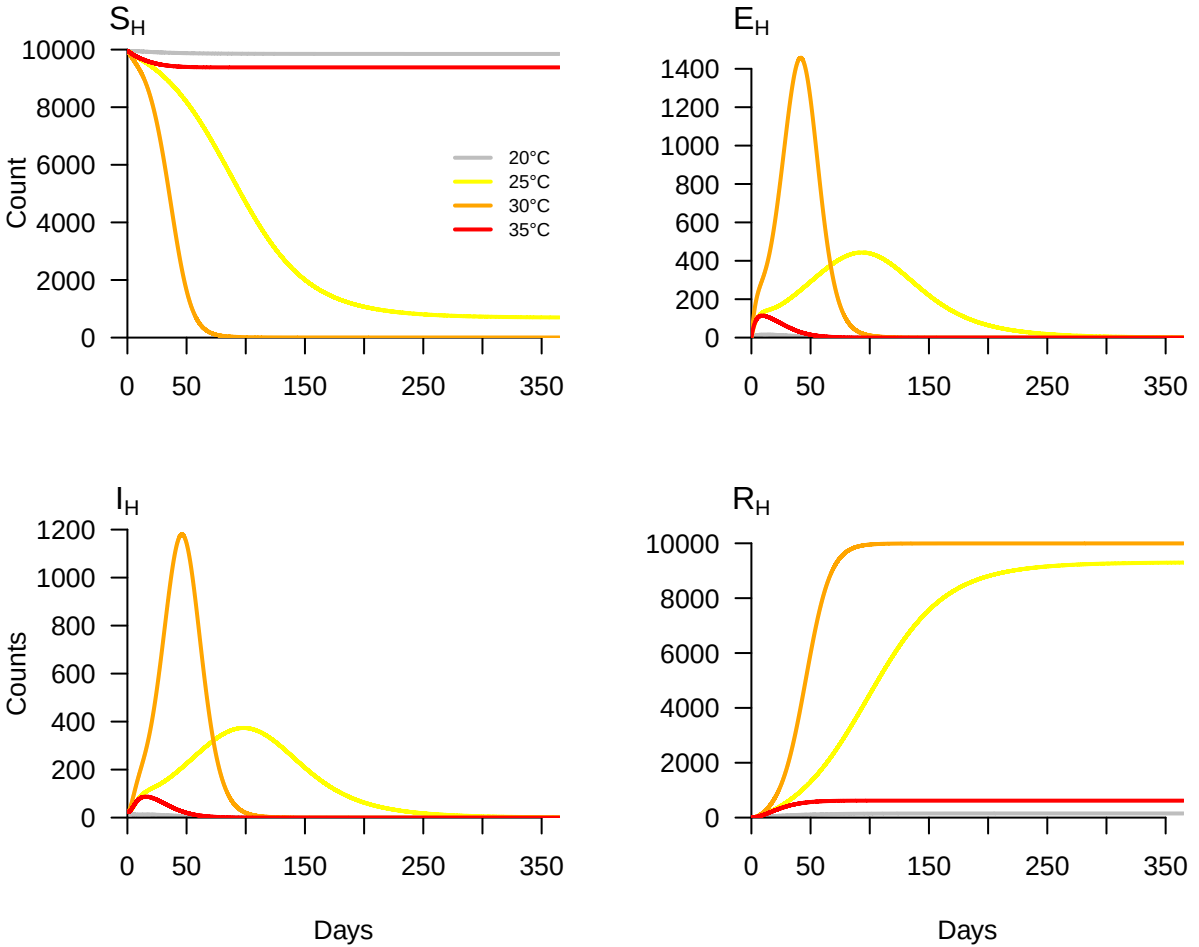
S_H
E_H
I_H
R_H
Count
Counts
Days
Days
20°C
25°C
30°C
35°C
0
2000
4000
6000
8000
10000
200
400
600
800
1000
1200
1400
0
50
150
250
350

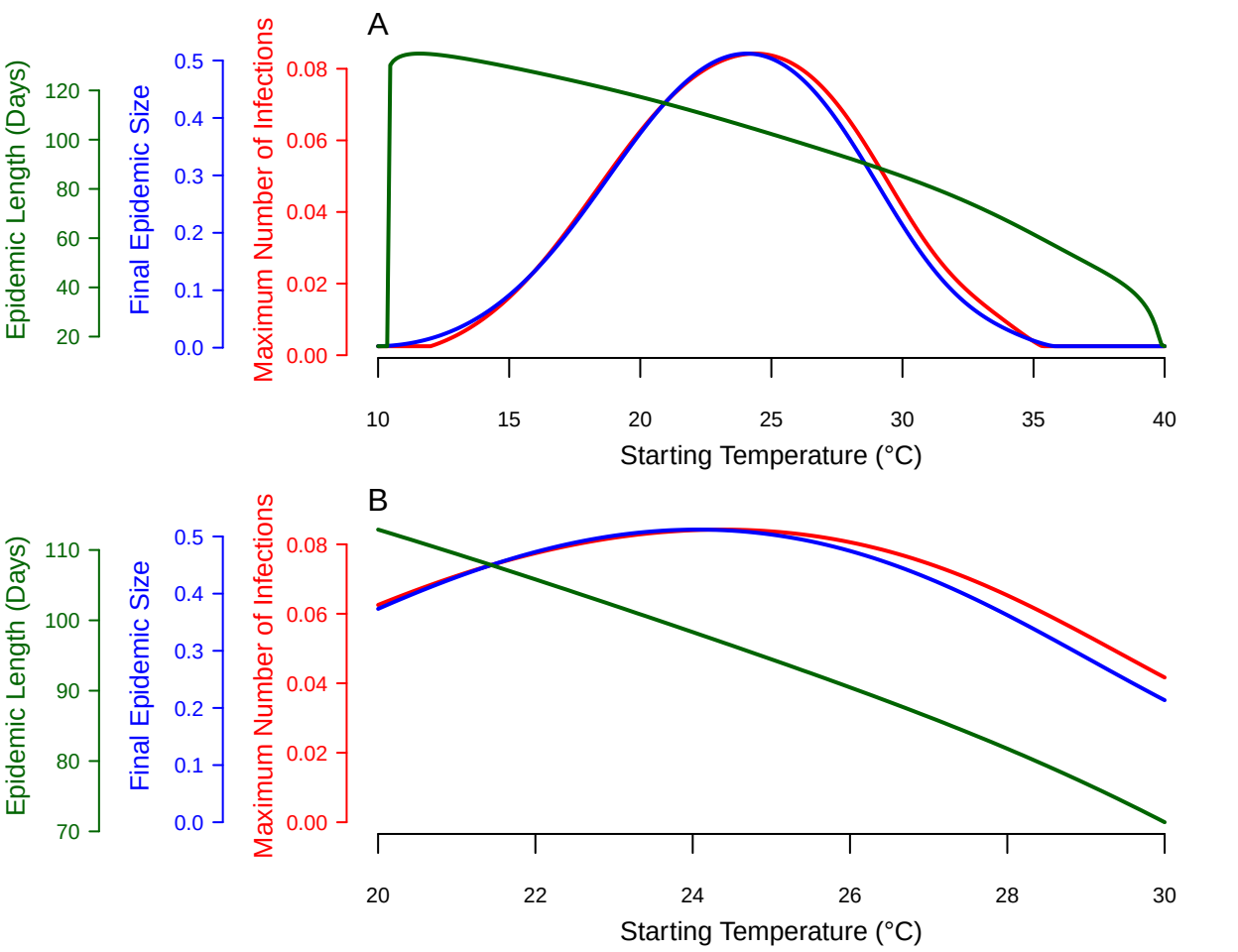
A
Epidemic Length (Days)
120
100
80
60
40
20
Final Epidemic Size
0.5
0.4
0.3
0.2
0.1
0.0
Maximum Number of Infections
0.08
0.06
0.04
0.02
0.00
10
15
20
25
30
35
40
Starting Temperature (°C)
B
Epidemic Length (Days)
110
100
90
80
70
Final Epidemic Size
0.5
0.4
0.3
0.2
0.1
0.0
Maximum Number of Infections
0.08
0.06
0.04
0.02
0.00
20
22
24
26
28
30
Starting Temperature (°C)

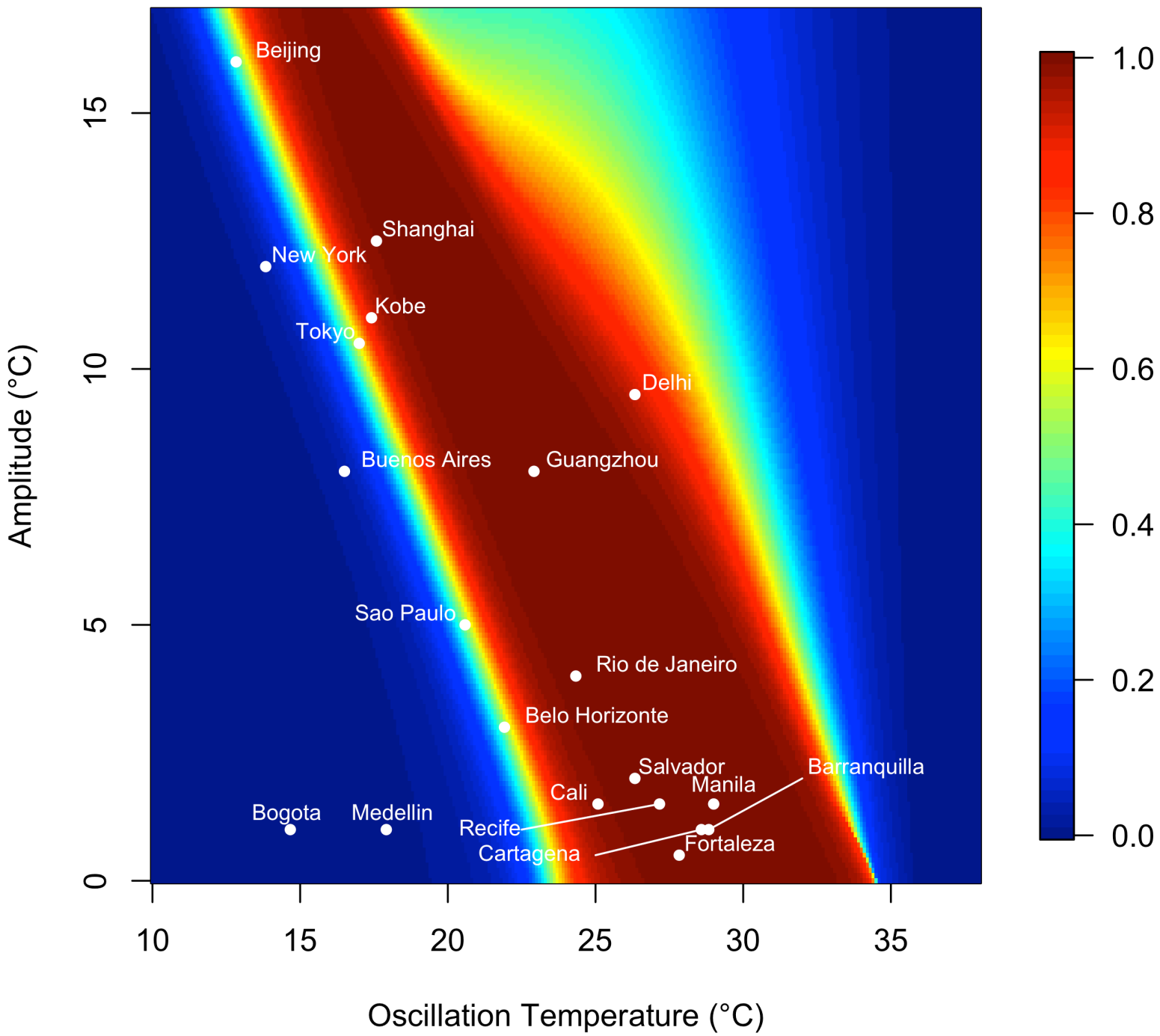
Beijing
Shanghai
New York
Kobe
Tokyo
Delhi
Buenos Aires
Guangzhou
Sao Paulo
Rio de Janeiro
Belo Horizonte
Salvador
Barranquilla
Manila
Cali
Bogota
Medellin
Recife
Cartagena
Fortaleza
Amplitude (°C)
0
5
10
15
10
15
20
25
30
35
Oscillation Temperature (°C)
1.0
0.8
0.6
0.4
0.2
0.0

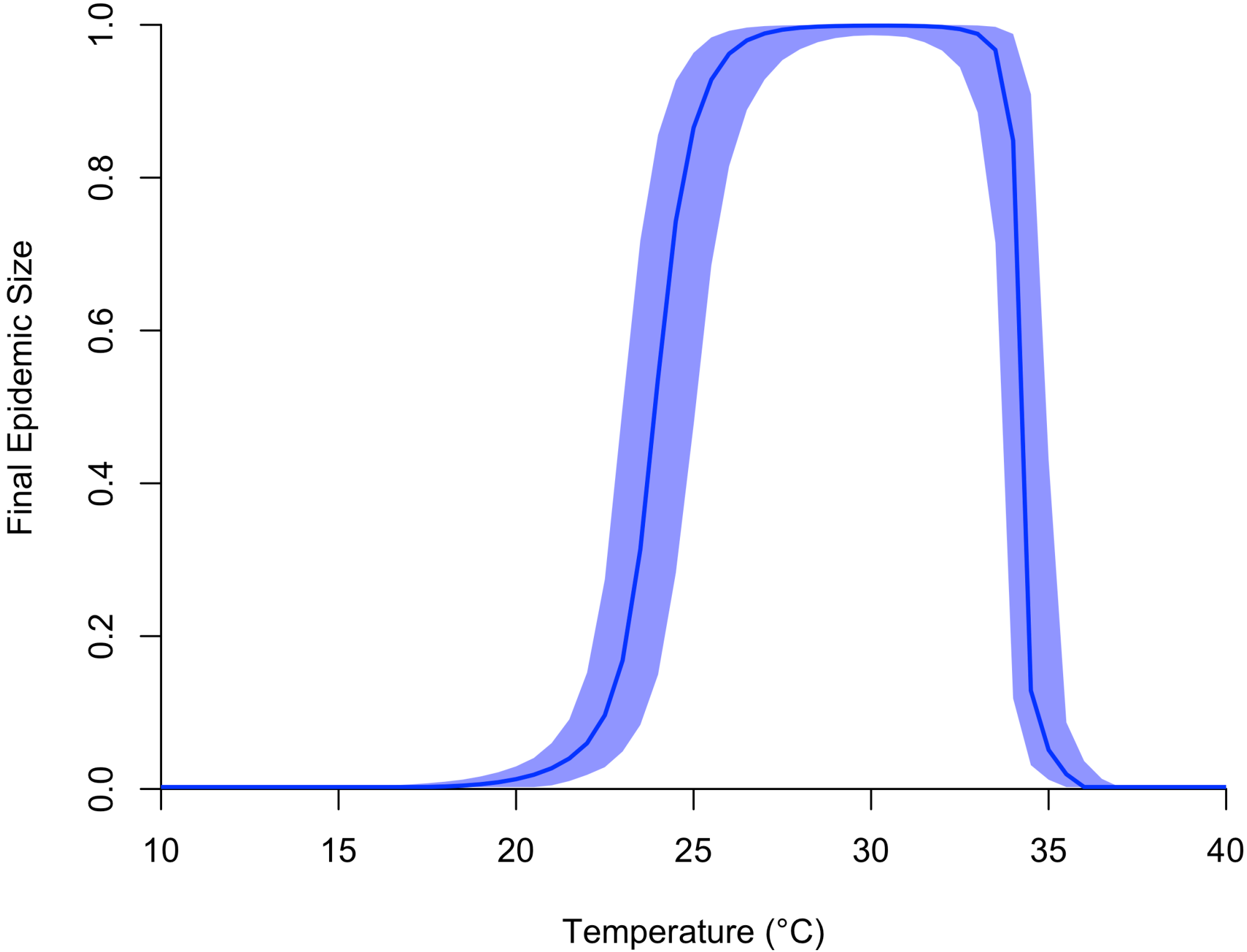
Final Epidemic Size
0.0
0.2
0.4
0.6
0.8
1.0
10
15
20
25
30
35
40
Temperature (°C)